Oxide Wizard: an EELS Application to Quantitatively Characterize the Oxidation State of Transition Metals

Oxide Wizard: Oxidation State of Transition Metals

Lluís Yedra[1,2], Elena Xuriguera[3], Marta Estrader[4], Alberto López-Ortega[5], M.D. Baró[6], Josep Nogués[7,8], Manuel Roldan[10,9], Maria Varela[9,10], Sònia Estradé[1,2] and Francesca Peiró[1]*

[1] Laboratory of Electron Nanoscopies (LENS)- MIND/IN2UB, Dept. d'Electrònica, Universitat de Barcelona, C/Martí i Franquès 1, E-08028 Barcelona, Spain.

[2] CCiT, Scientific and Technical Centers, Universitat de Barcelona, C/Lluís Solé i Sabaris 1, E-08028 Barcelona, Spain.

[3]Ciència de Materials i Enginyeria Metal·lúrgica, Dept. d'Enginyeria Química, Universitat de Barcelona, E-08028 Barcelona, Spain.

[4] Departament de Química Inorgànica, Universitat de Barcelona, Diagonal 645, E-08028, Barcelona, Spain.

[5] INSTM and Dipartimento di Chimica "U. Schiff", Università degli Studi di Firenze, Via della Lastruccia 3, Sesto Fiorentino, I-50019 Firenze, Italy

[6] Departament de Física, Universitat Autònoma de Barcelona, E-08193 Bellaterra (Barcelona), Spain.

[7] ICN2 – Institut Catala de Nanociencia i Nanotecnologia, Campus UAB, E-08193 Bellaterra (Barcelona), Spain.

[8]Institució Catalana de Recerca i Estudis Avançats (ICREA), Barcelona, Spain

[9]Materials Science & Technology Division, Oak Ridge National Laboratory, Oak Ridge, TN 37831, USA.

[10]Departamento de Física Aplicada III & Instituto Pluridisciplinar, Universidad Complutense de Madrid, E-28040 Madrid, Spain.

*Corresponding author: email: llyedra@el.ub.edu

The physicochemical properties of transition metal oxides are directly determined by the oxidation state of the metallic cations. To address the increasing need to accurately evaluate the oxidation states of transition metal oxide systems at the nanoscale, here we present 'Oxide Wizard'. This script for Digital Micrograph characterizes the oxidation states based on the energy-loss near edge structure (ELNES) and the position of the transition metal edges in the electron energy loss spectrum (EELS). This script allows the quantitative determination of the oxidation states with high spatial resolution. The power of the script is demonstrated by mapping manganese oxidation states in Fe_3O_4/Mn_3O_4 core/shell nanoparticles with sub-nm resolution in real space.

Keywords: EELS, spectrum image, transition metal oxides, oxidation state, Digital Micrograph script, manganese oxide.

1. Introduction

Transition metal (TM) oxides have maintained the interest of researchers during decades due to their appealing physiochemical properties, which have resulted in many different applications in a broad variety of fields. Interestingly,

many of these properties stem directly from their numerous possible oxidation states. Manganite perovskites, for example, have attracted much attention for their colossal magnetoresistance (CMR) properties which enable applications such as magnetoresistive tunnel junctions (Sun *et al.,* 1997). Actually, CMR is closely related to the electronic inhomogeneity and double exchange ensuing from the Mn^{+3}/Mn^{+4} mixed valence present in some doped manganites. Other fields where the TM valence is of great importance include mineralogy (van Aken *et al.,* 1995; Cave *et al.,* 2006; Loomer *et al.,* 2007; Zhang *et al.,* 2010), catalysis (Suchorski *et al.,* 2005), electro-chemistry (Graetz *et al.,* 2004) or 2D superconducting materials (Logvenov *et al.,* 2009) among many others.

The oxidation state can be defined as the number of electrons a given atom contributes to the bond, i.e. the hypothetical charge the atom would have in a purely ionic picture (McNaught & Wilkinson, 1997), and it is directly linked to the occupation of the 3d energy bands near the Fermi level of the material. However, the formal oxidation state differs from the actual charge on the TM atom (Luo *et al.,* 2007), as the bonds have a marked covalent character.

Importantly, for the accurate characterization of complex TM oxides and to properly understand their functional properties, measuring the oxidation state, i.e. the 3d band occupation, is of vital importance. Electron energy-loss spectroscopy (EELS) has been routinely used in order to obtain information on this electronic property, and there are a vast number of publications about the link between the oxidation state and the energy-loss near-edge structure (ELNES) of the $L_{2,3}$ edges ($2p \rightarrow 3d-$ like transitions) (Rask *et al.,* 1987; Paterson & Krivanek, 1990; Colliex *et al.,* 1991; Garvie & Craven, 1994; Garvie & Buseck, 1998; Botton *et al.,* 1995; Wang *et al.,* 2001; Daulton *et al.,* 2002;

Turquat *et al.,* 2001; Gloter *et al.,* 2001; Cave *et al.,* 2006; Kourkoutis *et al.,* 2006; Schmid & Mader*,* 2006; Riedl *et al.,* 2006; Meneses *et al.,* 2007; Loomer *et al.,* 2007; Riedl *et al.,* 2007; Riedl *et al.,* 2008; Arevalo-Lopez *et al.,* 2009; Varela *et al.,* 2009). Many methods have been reported to relate the $L_{2,3}$ ELNES and oxidation state, mainly through the measurements of L_{23} intensity ratios. However, most of these methods are not reliable when the signal-to-noise ratio (SNR) is poor, as is typically the case in 2D EEL spectrum images with short acquisition times per pixel. Here, we present Oxide Wizard, a script for Digital Micrograph which characterizes the shape and position of the transition metal edge and reliably produces maps of the 3d metal oxidation state.

2. Background, materials and methods

2.1 Background

Given the importance of the accurate determination of oxidation state in these materials, several procedures exist in order to correlate the features in the ELNES of the TM absorption edges with the oxidation state. Here we describe some of those procedures, based on the analysis of the $L_{2,3}$ edge or the O *K* edge observed in a typical EELS spectrum as in Fig. 1, which are already reported in the literature:

- *White line ratio:* in the case of TMs there are two clear peaks near the $L_{2,3}$ edge onset. These are the so-called white lines (WL), its name arising from the fact that they appeared as bright, overexposed stripes in X-rays and still appear as bright stripes in EEL spectra (Leapman *et al.,* 1982). They originate in transitions from the 2p to the 3d bands and their separation

corresponds to the spin-orbit splitting from the ground states of the transition ($2p_{3/2} \rightarrow 3d$) and ($2p_{1/2} \rightarrow 3d$). Intuitively, the ratio between the two peaks should correspond as well to the occupation of the ground states (2:1) if the final density of states was the same for all electrons. Experimentally, this is not observed although in many cases, and the changes in the ratio have been successfully related to oxidation states (van Aken *et al.,* 1998; Graetz *et al.,* 2004; Schmid *& Mader,* 2006; Riedl *et al.,* 2006; Varela *et al.,* 2009). There are several methods for extracting the WL intensities. Amongst them, the Pearson or step function method (Pearson *et al.,* 1993; Estrade *et al.,* 2012), where a linear model of the continuum is subtracted. The measurement of the L_{23} intensity ratios has been one of the most used techniques for oxidation state investigations, but it is very important to keep in mind that other characteristics than oxidation state, such as spin state, coordination geometry and ligand types, may play an important role (Daulton *et al.,* 2002; Gilbert *et al.,* 2003). Moreover, WL ratio increases with increasing thickness of the sample, but this effect can be removed by deconvolution of the low-loss spectrum (Tan *et al.,* 2012). Methods based on the second derivative (Botton *et al., 1995*) have also been used.

- *TM L edge onset (chemical shift):* the onset of edges will roughly correspond to the lowest energy of the final state. The position of the edge will change with changes in binding energy of the core level. In general, the edges move to higher energies for higher oxidation states (Tafto & Krivanek, 1982; Rask *et al.,* 1987; Daulton *et al.,* 2002; Gilbert *et al.,* 2003; Riedl *et al.,* 2007;,). This energy shift is usually referred to as chemical shift (Egerton R. F., 1996).

- *O K onset:* even if the nominal oxidation state of oxygen atoms is -2, the position of the *K* edge can be substantially different for different

compounds. In manganese compounds, the position of the oxygen *K* edge moves monotonically to lower energies for higher oxidation states of the cation (Gilbert *et al.,* 2003; Laffont & Gibot, 2010; Tan *et al.,* 2012), but this trend is not maintained for all TM oxides.

- *L_3 FWHM*: two important aspects influence the width of the L_3 peak: the oxidation state and the mixture of oxidation states. A slight change in the width of the peak with oxidation state was shown by Riedl *et al.* (Riedl *et al.,* 2007) while it had previously been calculated by Sherman (Sherman, 1984) and Kurata and Colliex (Kurata & Colliex, 1993). However, the sensitivity to the oxidation state is very low, around 20% as calculated by Riedl with good SNR. However, the width of the peak contains information about mixed valences. The $L_{2,3}$ edges for materials containing TMs in different oxidation states can be regarded as the superposition of two edges of the different oxidation states rather than a single edge of the average valence.

- *TM L to O K energy distance*: taking into account that the oxygen *K* edge onset and that of the TM both shift, the relative distance between the two of them is an interesting feature of the spectrum when no absolute energy positions can be determined. This quantity is related to the energy difference between the 1*s* level of the oxygen and the $2p_{3/2}$ level of the TM. While it may be equivalent to the TM edge onset if the O 1*s* state remains the same (Arevalo-Lopez *et al.,* 2009), this quantity is generally different due to the non-monotonicity between the oxidation state and the O *K* edge position. This feature is still particularly useful when no absolute positions can be determined.

- *L_2-L_3 energy distance*: the difference in energy between the L_3 and the L_2 peaks is a feature rarely used in previous work. The separation of the peaks arises from the spin-orbit splitting from the ground states of the

transitions $(2p_{3/2} \rightarrow 3d)$ and $(2p_{1/2} \rightarrow 3d)$. Therefore, any change in the separation is related with the changes in the ground states.

- *O K peak-separation method:* The energy separation between the O *K* pre-peak and the edge main peak is a highly successful and accurate approach to measure oxidation states, which has been tested both experimentally (Varela *et al.,* 2009) and (Luo *et al.,* 2009). This method, however, is difficult to use in complex heterosystems such as interfaces between two oxides due to beam broadening and cross-talk effects.

All these methods yield consistent results when used on data with good SNR. However, a good SNR is hardly found when working with complex data sets such as two dimensional spectrum images. Thanks to the recent advances in electron microscopes (Gubbens *et al.,* 2010) the number of spectra available in a single spectrum image (SI) is rapidly increasing. Therefore, a procedure to extract reliable oxidation state information from a great number of spectra at a time is needed. In order to address this need, we have developed the Oxide Wizard software, an automated routine for Gatan Digital Micrograph (DM). As we will show, our approach offers a method for characterizing the white lines of transition metals in a reproducible, reliable manner, including all the necessary tools in a single interface.

2.2. Materials and methods

To demonstrate the power of the script we have studied the Mn oxidation states in Fe_3O_4/Mn_3O_4 core/shell nanoparticles. The nanoparticles were grown

using the seeded-growth method (Salazar-Alvarez *et al.,* 2011, Lopez-Ortega *et al.,* 2012), the Mn-oxide layer was grown on Fe_3O_4 11 nm seeds by hot injection.

Importantly, to calibrate the script, bulk materials with known oxidation states are necessary. In our case, since we are interested in the Mn oxidation states, a number of different bulk manganese oxides (MnO, Mn_3O_4, Mn_2O_3 and MnO_2) were synthesized by our colleagues in Ciència de Materials i Enginyeria Metal·lúrgica in the department of chemical engineering of the University of Barcelona. The structure of the samples was confirmed by X-ray diffraction. The calibration was carried out in a Jeol JEM 2010F operated at 200kV and equipped with a Gatan GIF spectrometer.

EEL spectrum images of the nanoparticles studied where acquired in an aberration-corrected Nion UltraSTEM200 operated at 200 kV and equipped with a Gatan Enfinium spectrometer at Oak Ridge National Laboratory.

2.3. Steps of the analysis

The script, written in Digital Micrograph scripting language, is divided in several sequential steps which are summarized in the flow chart in Fig. 2.

The first three steps are optional and allow the user to improve the quality of the data to ease further analysis. The first step consists on the **deconvolution** of the low-loss region of the spectrum. Core-loss edges are usually broadened because of the effects of multiple scattering. If the sample is not thin enough, it is likely that the electrons suffering inelastic scattering will also undergo at least a plasmon excitation, broadening the ELNES and, hence,

changing the shape of the continuum. If the measurements are carried out in a thin specimen or in an area of the sample with constant thickness and only used for comparison purposes, low-loss deconvolution is not necessary. Otherwise, deconvolution of the low-loss region is typically required. This step can be achieved using the Fourier ratio deconvolution already available in the DM EELS package. **Binning** can be achieved by summing spectra, and it can be helpful when the dataset is very noisy or when performing test runs on very large spectrum images.

Next, an **energy drift correction** procedure can be carried out. This step is based on the presence of other peaks other than the TM or the oxygen in the spectra. It consists on choosing an edge in one single spectrum with a region of interest (ROI) tool provided by the script. The energy drift is calculated using a cross correlation of that region of the reference spectrum and the rest of the spectra. A new, drift-corrected spectrum image is created. If it is not possible to use an edge other than the oxygen or the TM, drift correction is still useful. If the energy drift is too large, the adequate ROI for a single spectrum will be inadequate for the rest and the analysis can fail. The absolute peak position of the TM edge is lost if we apply the drift correction procedure on it, but the relative position to O *K* edge may still be valuable

Subsequently, the **onset of the oxygen *K* edge** is analyzed. The onset is located at the minimum of the rise. Choosing the first peak of the oxygen with a ROI, the onset is found as a minimum in a modified second derivative, equivalent to the second derivative filter in DM, where maxima in the original function correspond to maxima in the filtered version. The modification inverts

the second derivatives in order to locate maxima that correspond to minima in the actual second derivative of the function.

Finally, the **ELNES of the TM** is characterized by finding the positions of the maxima of the two white lines, the onset of the L_3, the minimum in between and the end of the L_2. It must be noticed that before this analysis the background needs to be subtracted (by using power-law fits in DM or other models). After placing a ROI on the white lines of a single spectrum, the script calculates the second derivative, finds the maximum and fits a Gaussian curve to it. This maximum corresponds to the first white line. This curve is then used to calculate the position of the by cross correlating it with the second derivative of the spectrum. A cross-correlation is used since it is easily and rapidly calculated in DM, and it is robust against noise and it enhances actual white line peaks in the second derivative against local maxima and minima.

The cross-correlation has a few distinct features: a global maximum placed at zero position and a series of peaks which match the greater features of the second derivative of the spectrum. The minimum before the first white line is taken as the onset of the edge. The global maximum not corresponding to the zero position, found as the maximum of the cross-correlation after a few eV from the zero, corresponds to the second white line. The two other features are less important for the analysis, but are calculated anyway for further data treatment. The valley between the WL and the end of the ELNES are found as the minima after the first and second white lines respectively. The result can be used to detect any error in the peak detection.

Once the features of the ELNES are located, we already have the information about the absolute positions of the lines. However, if we want to

integrate the areas under the peaks, it is necessary to remove the contribution of the continuum (Pearson *et al.,* 1993). A few methods have been devised for this purpose, such as modeling it with Hartree-Slater cross sections. This method calculates the continuum contribution with a neutral atom cross section. However, a simpler alternative is a linear fitting of the continuum, i.e., the Pearson method, which has been chosen for its simplicity and for having results similar to those of Walsh Dray (Pearson *et al.,* 1993). For this method, the continuum is modeled as a two step function with the steps centered under the peaks, with a height ratio of 2:1 from first to second and with a slope calculated by a linear fit of the continuum after the peaks. This function is subtracted from the data before the intensity under the peaks is calculated. The script allows the user to decide the width of the integrating windows and also the continuum modeling region.

The script can present the results for a single spectrum or for the whole spectrum image. In both cases the results can be refined by fitting the peaks after the continuum subtraction with two Gaussian curves. The final results provided by the script are the TM edge onset, the white line L_{23} ratio, the energy split between the two WLs, the energy between the O *K* and the TM $L_{2,3}$ edge and the FWHM of the first WL.

3. Results

3.1. Calibration test on Mn_xO_y oxides

In Figure 3, single spectra for the four different bulk manganese oxides considered (MnO, Mn_3O_4, Mn_2O_3 and MnO_2) are shown. The differences in the

O *K* edges and the Mn $L_{2,3}$ edges are clear, the L_3/L_2 ratio decreases with oxidation state and the O *K* onset position increases. Rather than calibration curves, we have preferred the two-parameter method introduced by Daulton (Daulton *et al.,* 2002) in chromium and performed by Tan on manganese and iron oxides (Tan *et al.,* 2012). This method presents the results of the two WL features in the same plot. While a single parameter can be misleading, the two-parameter method makes the characterization easier. The results of this procedure are plotted as two-parameter charts in Figure 4. The Mn $L_{2,3}$ onset is discarded, as there was no absolute measure of the position. Similarly, the L_3 – L_2 distance is not used since it did not show relevant changes in the data. The white line ratio did show the expected changes, and in Figure 4a it is plotted against the O *K* to Mn L_3 distances, which also showed a large change between oxidation states. In the chart, although the different formal oxidation states are separated, the Mn_3O_4 (in red) and Mn_2O_3 (in blue) show data clouds very close to one another, with some data points overlapping. To avoid ambiguity in the analysis, a third parameter, FWHM of L_3 peak, is introduced. As it can be clearly seen in Figure 4b, in this case all the data clouds, and particularly Mn_3O_4 and Mn_2O_3 ones, are well separated.

Mn_2O_3 has a single oxidation state, with Mn^{3+}, while Mn_3O_4 contains a mixture of Mn^{3+} and Mn^{2+} in a two-to-one ratio. The measured edge can be seen as a superposition of both oxidation states. The onset of the edge for Mn_3O_4 is, therefore close to that of the Mn_2O_3 edge, both given by the Mn^{3+} contribution. However, there was a variation in O *K* position, so the distance between O and Mn edges showed a change. The white line ratio is also very close for the two

compositions. However, the FWHM of the mixed oxide is expected to be larger, since the L_3 will be a superposition of two displaced peaks. The experimental results corroborate this point.

3.2. Mn oxidation state determination application

Once the parameters for the edges of the diverse manganese oxide reference materials have been established, the routine can be applied to a sample of unknown oxidation state. The sample consists of core-shell nanoparticles, where the core corresponds to an iron oxide and the shell to a manganese oxide. A high angle annular dark field (HAADF) image of a nanoparticle is shown in Figure 5a. In this image, the core and the inhomogeneous shell are difficult to tell apart. If we carry out a multiple linear least squares (MLLS) fitting of the EELS spectrum image for the iron and manganese edges, we can obtain a composite image with compositional contrast, as shown in Figure 5b. In this figure, the iron oxide core appears as a round particle presented in red, while the manganese oxide grows as discontinuous crystallites around the core (in green).

The spectrum image has been fitted to two single spectra in Fig. 6a from the surface (orange) and the inner part (blue) of the Mn oxide shell. The two spectra had different characteristics, pointing to different oxidation states. The red spectrum, extracted from the surface region has higher WL ratio, a thinner L_3 and with an onset shifted to lower energies than the green spectrum extracted from the inner parts of the manganese oxide shell. The result of the fitting is shown in Fig. 6b, where we can observe a distribution of manganese

oxidation states. However, the MLLS fitting maps only offer qualitative information if we do not have more prior information about the sample. We then apply OW to quantify the results.

The spectra were rather noisy, so multivariate analysis was applied prior to OW. This kind of analysis will be explained next. The script has been applied to the whole spectrum image, consisting on 100x70 single spectra as the one shown in Fig. 5c, both with and without low-loss deconvolution, The differences in both procedures were negligible, mainly due to the small thickness of the particle, which, along with the carbon support summed only 0.3 inelastic mean free paths. The results of the deconvolved spectra are shown in Fig.7. The Mn white line ratio (Fig. 7a) in the particle ranges from 3 to 3.5. The FWHM of the L_3 line (Fig. 7b) has values between 4 and 6 eV, and the energy separation between the O *K* edge and the Mn $L_{2,3}$ (Fig. 7c) goes from 112 to 115 eV.

4. Discussion

In the manganese oxide shell, two different regions can be seen, corresponding to the surface and the inner areas of the shell. At the surface, the values of both the WL ratio (3.5) and the O-Mn distance (112 eV) point to a MnO-like composition according to the two parameter chart in Fig. 4 with an oxidation state of Mn^{2+}. In the inner regions of the shell, displayed in green in Fig. 7a and in the range green to yellow in Fig. 7b, the WL ratio is around 3, and the O-Mn distance is around 115 eV. In Fig.4, however, these values do not correspond to any of the reference oxidation states. The values lie between Mn^{2+}

and $Mn^{2.66+}$. The spectra for the inner regions of the manganese oxide result from a superposition of the inner and outer areas, as the electron travels through the entire thickness of the sample. Therefore, the actual oxidation state in the inner part must be higher than measured. Using the FWHM measurements, the differences between the surface and the interior of the manganese regions is of 2 eV, the same difference found between Mn^{2+} and $Mn^{2.66+}$. Therefore, we can assume that the oxidation state of manganese ranges from Mn^{2+} at the surface to $Mn^{2.66+}$ in the inside. Interestingly, in our bulk compounds a nominal oxidation state of +2.66 would on average be found in Mn_3O_4. Consequently, our results indicate than the shell of the particles may be composed by an inhomogeneous Mn oxide, with a mixture of MnO at the surface and Mn_3O_4 rich areas within the shells.

5. Conclusions

A script for Digital Micrograph, Oxide Wizard, has been developed to characterize the white lines found in the ELNES of transition metals, dealing with large spectrum images in a systematic, reproducible, way. As an output, the script plots the white line ratio, the oxygen *K* edge onset, the TM edge onset, the difference between both, the FWHM of the TM first WL and the separation of the WLs. From these parameters, and using the WLs reference compounds, quantitative information on the oxidation state of the samples can be easily obtained. This procedure has been applied to iron oxide/manganese oxide

core/shell nanoparticles with unknown manganese oxidation states. The results evidence, with sub-nm resolution, the existence nano-domains with distinct oxidation states consistent with the presence of Mn_3O_4 in the interior of the shell and MnO rich regions near its surface. Hence, Oxide Wizard has been demonstrated to be very effective and reliable script capable of dealing with large datasets that permits real time processing of data within the Digital Micrograph interface.

ACKNOWLEDGEMENTS: Research at ORNL (MV) was sponsored by the Materials Sciences and Engineering Division of the U.S. Department of Energy (DOE). Research at UCM sponsored by the ERC starting Investigator Award, grant #239739 STEMOX. The authors acknowledge the financial support of the 2009-SGR-1292 and 2009 SGR 00035 projects of the Generalitat de Catalunya and the MAT2010-20616-C02, MAT2010-16407 and 2009CSD-00013 projects of the Spanish Ministry of Science and Innovation (MICINN)

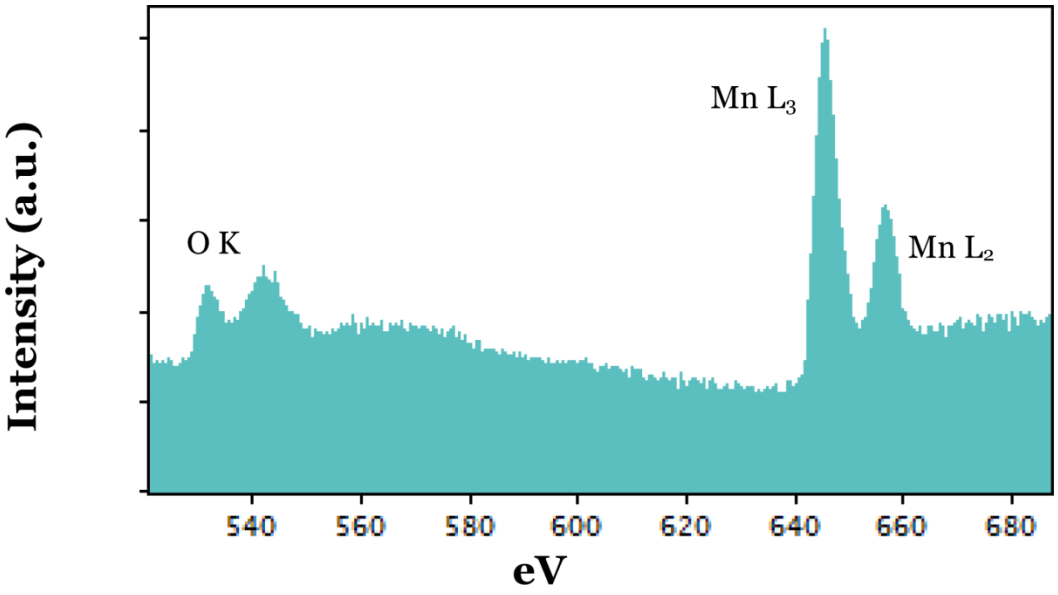

Figure 1: Single spectrum of a manganese oxide, including the oxygen *K* edge and the Mn $L_{2,3}$ white lines.

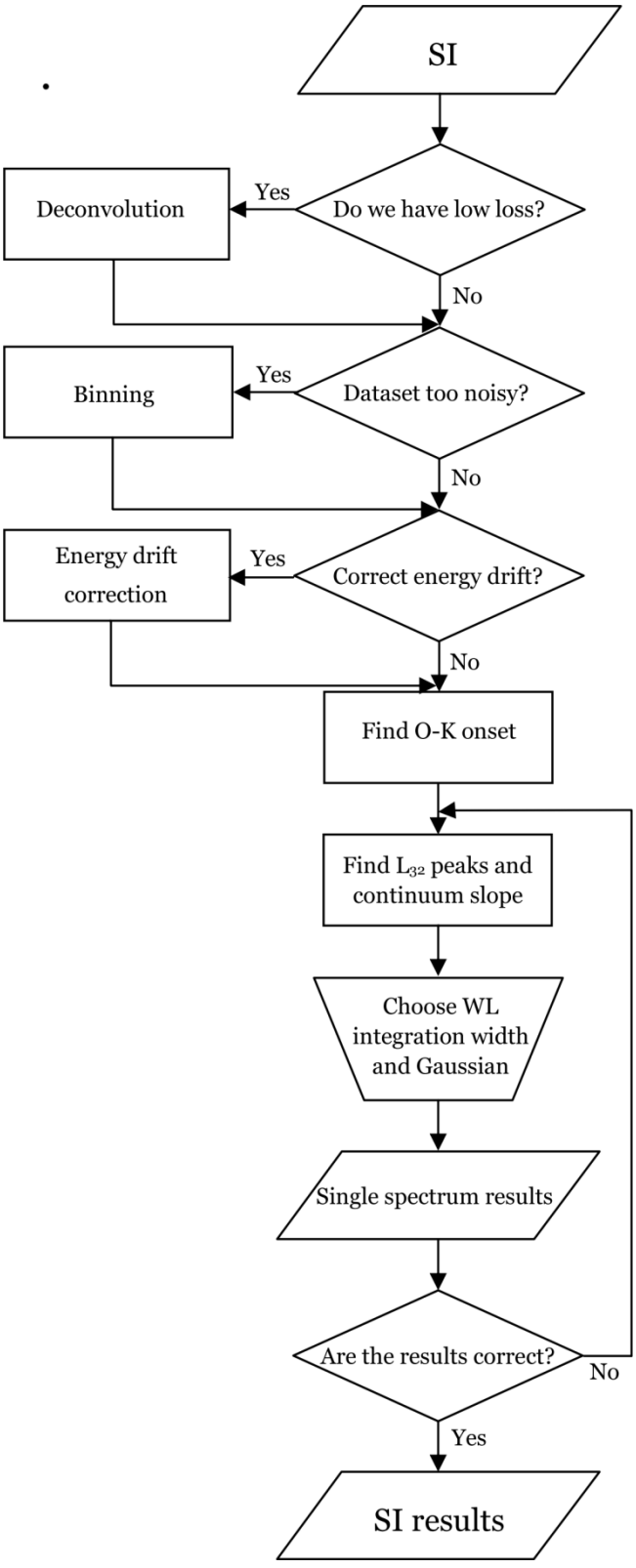

Figure 2: Flow chart of the script, starting with a spectrum image and ending in the results.

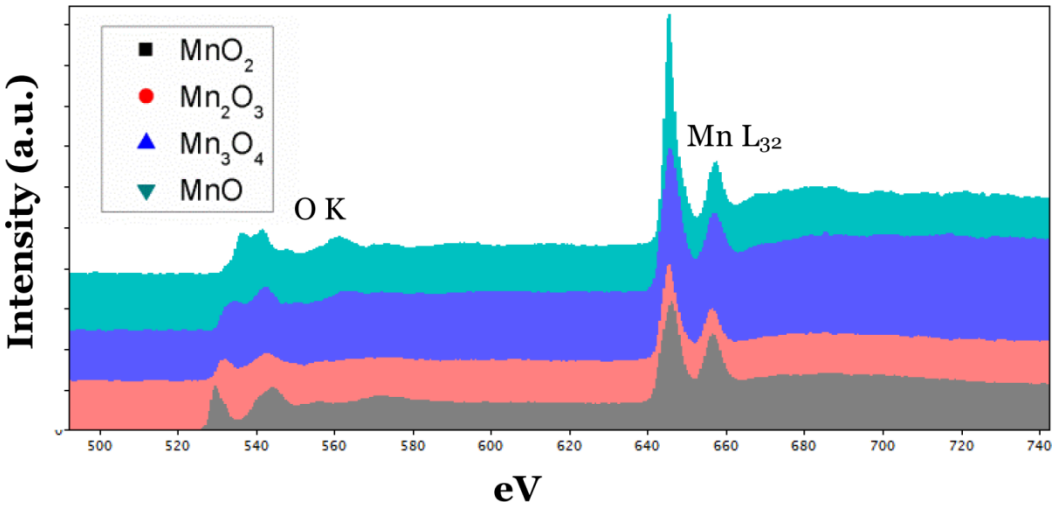

Figure 3: Single spectra of the different manganese oxide reference materials used for data extraction for Mn formal oxidation ratios ranging from 2 to 4, displaced in the intensity direction. The spectra are aligned at the Mn $L_{2,3}$ edge.

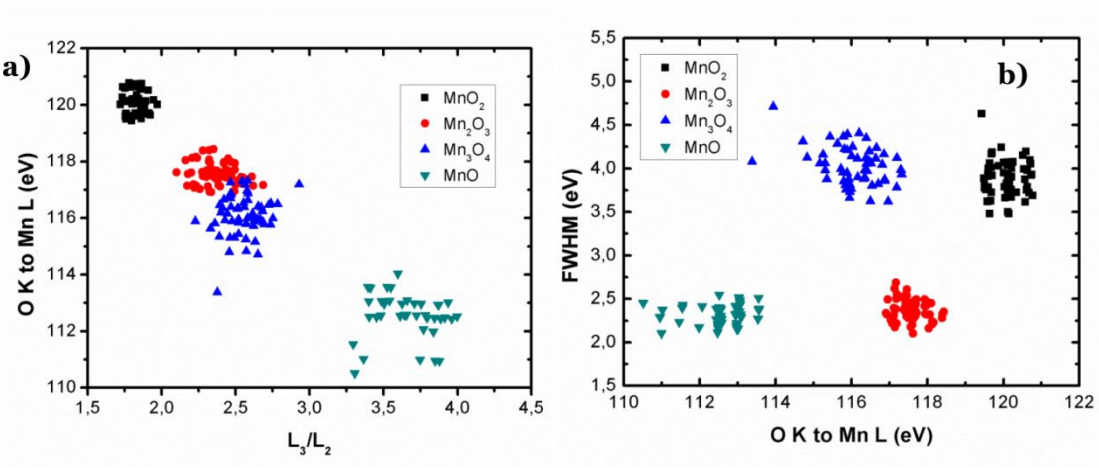

Figure 4: Two-parameter chart combining **a)** white line ratios and O *K* to Mn L_3 distances and **b)** O *K* to Mn L_3 distances and FWHM of the L_3 peak for Mn formal oxidation ratios ranging from 2 to 4.

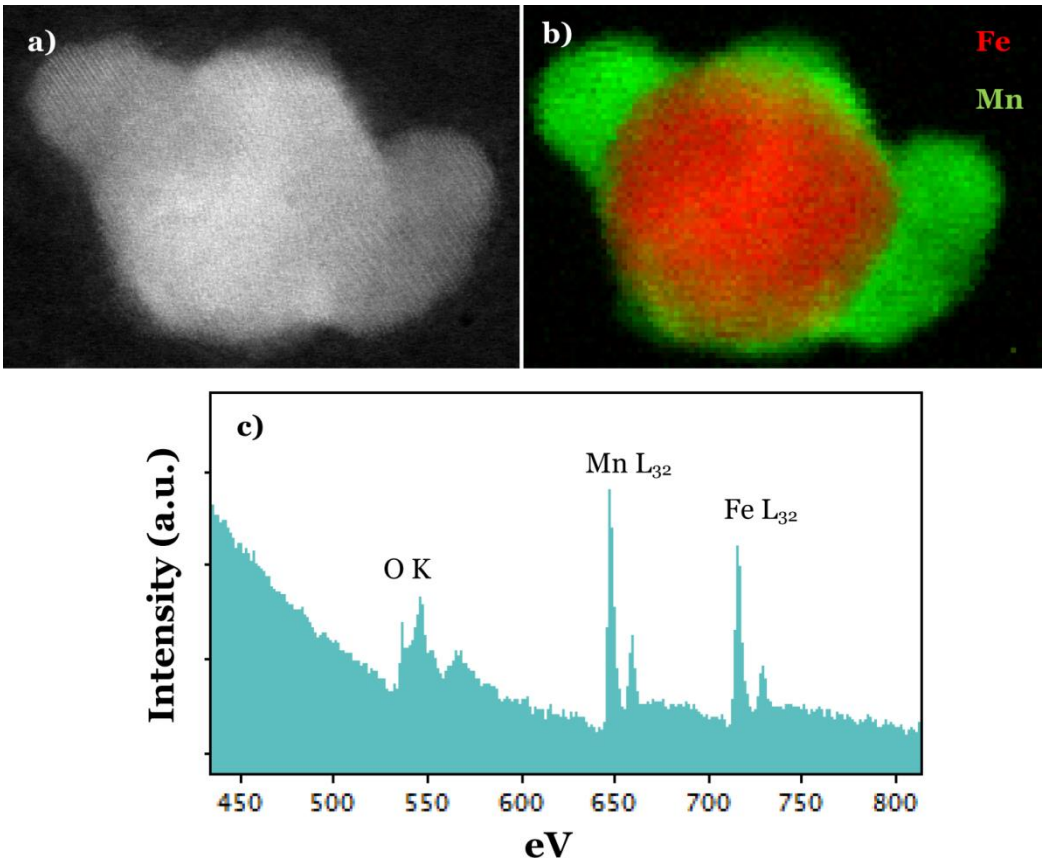

Figure 5: a) HAADF image of the particle and **b)** composite image of MLLS fitting of the spectrum image to the iron and manganese *L* edges. **c)** Single spectrum showing the oxygen *K*, manganese $L_{2,3}$ and iron $L_{2,3}$ edges.

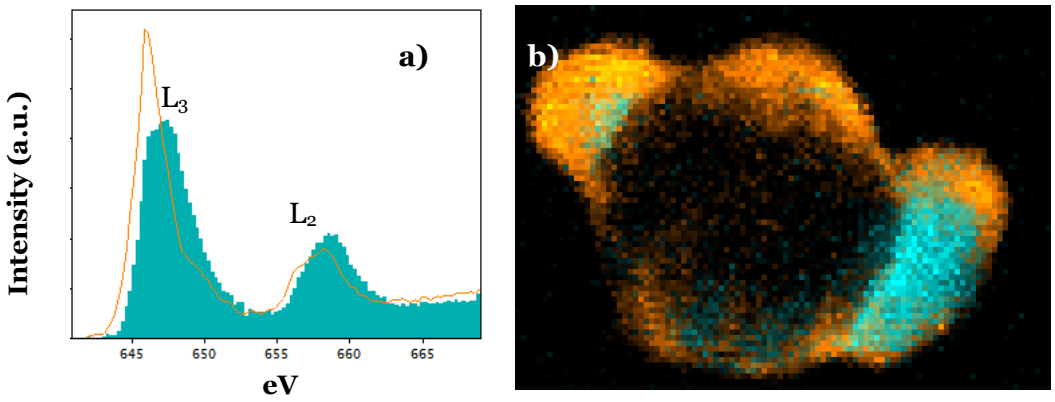

Figure 6: a) Mn $L_{2,3}$ edges extracted from the border (in orange) and the inner area (in turquoise) of the manganese oxide shell and **b)** composite image of MLLS fitting of the spectrum image to the two spectra in **a**.

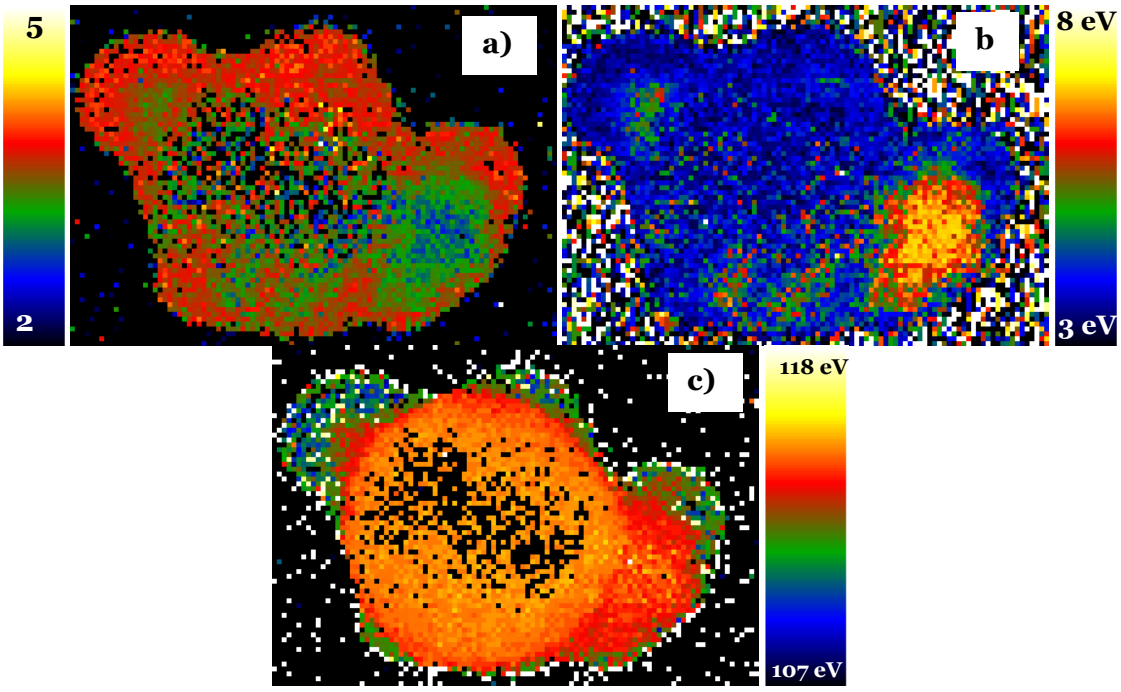

Figure 7: Different outputs of the Oxide Wizard script: **a)** WL ratio. **b)** L_3 FWHM after Gaussian fitting. **c)** O *K* to Mn L_3 distance.

References

AREVALO-LOPEZ, A. M. and ALARIO-FRANCO M. A. (2009). Reliable Method for Determining the Oxidation State in Chromium Oxides. *Inorg. Chem.* **48,** 11843-11846.

BOTTON, G. A., APPEL, C. C., HORSEWELL, A. & STOBBS, W. M. (1995). Quantification of the EELS near-edge structures to study Mn doping in oxides. *Journal of Microscopy-Oxford* **180,** 211-216.

CAVE, L., AL, T., LOOMER, D., COGSWELL, S. & WEAVER L. (2006). A STEM/EELS method for mapping iron valence ratios in oxide minerals. *Micron* **37,** 301-309.

COLLIEX, C., MANOUBI, T. & ORTIZ, C. (1991). Electron-Energy-Loss-Spectroscopy Near-Edge Fine-Structures in the Iron-Oxygen System. *Physical Review B* **44,** 11402-11411.

DAULTON, T. L., LITTLE, B. J., LOWE, K. & JONES-MEEHAN, J. (2002). Electron energy loss spectroscopy techniques for the study of microbial chromium (VI) reduction. *J. Microbiol. Methods* **50,** 39-54.

EGERTON, R. F. (1996). *Electron Energy-Loss Spectroscopy in the Electron Microscope*; New York, USA: Plenum Press.

ESTRADE, S., YEDRA, L., LOPEZ-ORTEGA, A., ESTRADER, M., SALAZAR-ALVAREZ, G., BARO, M. D., NOGUES, J. & PEIRO, F. (2012), Distinguishing the core from the shell in MnO_x/MnO_y and FeO_x/MnO_x core/shell nanoparticles through quantitative electron energy loss spectroscopy (EELS) analysis. *Micron* **43,** 30-36.

GARVIE, L. and CRAVEN, A. (1994). High-Resolution Parallel Electron-Energy-Loss Spectroscopy of Mn L(2,3)-Edges in Inorganic Manganese Compounds. *Phys. Chem. Miner.* **21,** 191-206.

GARVIE, L. A. J. and BUSECK, P. R. (1998). Ratios of ferrous to ferric iron from nanometre-sized areas in minerals. *Nature* **396,** 667-670.

GILBERT, B., FRAZER, B., BELZ, A., CONRAD, P., NEALSON, K., HASKEL, D., LANG, J., SRAJER, G. & DE STASIO, G. (2003). Multiple scattering calculations of bonding and X-ray absorption spectroscopy of manganese oxides. *J. Phys Chem A* **107,** 2839-2847.

GLOTER, A., SERIN, V., TURQUAT, C., CESARI, C., LEROUX, C. & NIHOUL, G. (2001). Vanadium valency and hybridization in V-doped hafnia investigated by electron energy loss spectroscopy. *Eur. Phys. J. B* **22,** 179-186.

GRAETZ, J., AHN C., OUYANG, H., REZ, P. & FULTZ, B. (2004). White lines and d-band occupancy for the 3d transition-metal oxides and lithium transition-metal oxides. *Phys. Rev. B* **69,** 235103.

GUBBENS, A., BARFELS, M., TREVOR, C., TWESTEN, R., MOONEY, P., THOMAS, P., MENON, N., KRAUS, B., MAO, C. & MCGINN, B. (2010). The GIF Quantum, a next generation post-column imaging energy filter. *Ultramicroscopy* **110,** 962-970.

KOURKOUTIS, L. F., HOTTA, Y., SUSAKI, T., HWANG, H. Y. & MULLER, D. A. (2006). Nanometer scale electronic reconstruction at the interface between LaVO3 and $LaVO_4$. *Phys. Rev .Lett.* **97,** 256803.

KURATA, H. and COLLIEX, C. (1993). Electron-Energy-Loss Core-Edge Structures in Manganese Oxides *Phys. Rev. B* **48,** 2102-2108.

LAFFONT, L. and GIBOT, P. (2010). High resolution electron energy loss spectroscopy of manganese oxides: Application to Mn_3O_4 nanoparticles. *Mater. Charact.* **61,** 1268-1273.

LEAPMAN, R. D., GRUNES, L. A. & FEJES, P. L. (1982). Study of the L_{23} edges in the 3d transition metals and their oxides by electron-energy-loss spectroscopy with comparisons to theory. *Phys. Rev. B* **26,** 614-635.

LOGVENOV, G., GOZAR, A. & BOZOVIC, I. (2009). High-Temperature Superconductivity in a Single Copper-Oxygen Plane. *Science* **326,** 699-702.

LOOMER, D. B., AL, T. A., WEAVER, L. & COGSWELL, S. (2007). Manganese valence imaging in Mn minerals at the nanoscale using STEM-EELS. *Am. Mineral.* **92,** 72-79.

LOPEZ-ORTEGA, A., ESTRADER, M., SALAZAR-ALVAREZ, G., ESTRADE, S., GOLOSOVSKY, I. V., DUMAS, R. K., KEAVNEY, D. J., VASILAKAKI, M., TROHIDOU, K. N., SORT, J., PEIRO, F., SURINACH, S., BARO, M. D. & NOGUES J. (2012). Strongly exchange coupled inverse ferrimagnetic soft/hard, $Mn_xFe_{3-x}O_4/Fe_xMn_{3-x}O_4$, core/shell heterostructured nanoparticles. *Nanoscale* **4,** 5138-5147.

LUO, W., VARELA, M., TAO, J., PENNYCOOK, S. J. & PANTELIDES S. T. (2009). Electronic and crystal-field effects in the fine structure of electron energy-loss spectra of manganites. *Physical Review B* **79,** 052405.

LUO, W., FRANCESCHETTI, A., VARELA, M., TAO, J., PENNYCOOK, S. J. & PANTELIDES, S. T. (2007). Orbital-occupancy versus charge ordering and the strength of electron correlations in electron-doped $CaMnO_3$. *Phys. Rev. Lett.* **99,** 036402.

MCNAUGHT, A. D. & WILKINSON, A. (1997). IUPAC. Compendium of Chemical Terminology (the "Gold Book"). Oxford, U.K. Blackwell Scientific Publications.

MENESES, C. T., VICENTIN, F. C., SASAKI, J. M. & MACEDO, M. A. (2007). Influence of Li on the K-edge of O and L-2,L-3 of the Mn XANES in $Li_xMn_2O_4$ thin films. *J. Electron Spectrosc. Rel. Phen.* **156,** 326-328.

PATERSON, J. H. and KRIVANEK, O. L. (1990). Elnes of 3d transition-metal oxides: II. Variations with oxidation state and crystal structure. *Ultramicroscopy* **32,** 319-325.

PEARSON, D. H., AHN, C. C. & FULTZ, B. (1993). White lines and d-electron occupancies for the 3d and 4d transition metals. *Phys. Rev. B* **47,** 8471.

RASK, J., MINER, B. & BUSECK, P. (1987). Determination of Manganese Oxidation-States in Solids by Electron Energy-Loss Spectroscopy. *Ultramicroscopy* **21,** 321-326.

RIEDL, T., GEMMING, T. & WETZIG, K. (2006). Extraction of EELS white-line intensities of manganese compounds: Methods, accuracy, and valence sensitivity. *Ultramicroscopy* **106,** 284-291.

RIEDL, T., GEMMING, T., GRUNER, W., ACKER, J. & WETZIG, K. (2007). Determination of manganese valency in $La_{1-x}Sr_xMnO_3$ using ELNES in the (S)TEM. *Micron* **38,** 224-230.

RIEDL, T., SERRA, R., CALMELS, L. & SERIN, V. (2008). Valence sensitivity of Fe-$L_{2,3}$ white-line ratios extracted from EELS. In *EMC 2008, Volume 1: Instrumentation and Methods*. M. Luysberg, K. Tillmann & Thomas Weirich (Eds.) pp. 419-420. Berlin, Germany: Springer-Verlag Berlin Heidelberg.

SALAZAR-ALVAREZ, G., LIDBAUM, H., LOPEZ-ORTEGA, A., ESTRADER, M., LEIFER, K., SORT, J., SURINACH, S., BARO, M. D. & NOGUES, J. (2011). Two-, Three-, and Four-Component Magnetic Multilayer Onion Nanoparticles Based on Iron Oxides and Manganese Oxides. *J. Am. Chem. Soc.* **133,** 16738-16741.

SCHMID, H. K. and MADER, W. (2006) Oxidation states of Mn and Fe in various compound oxide systems *Micron* **37,** 426-432.

SHERMAN, D. M. (1984). The Electronic-Structures of Manganese Oxide Minerals *Am. Mineral.* **69,** 788-799.

SUCHORSKI, Y., RIHKO-STRUCKMANN, L., KLOSE, F., YE, Y., ALANDJIYSKA, M., SUNDMACHER, K. & WEISS, H. (2005). Evolution of oxidation states in vanadium-based catalysts under conventional XPS conditions. *Appl. Surf. Sci.* **249,** 231-237.

SUN, J., KRUSINELBAUM, L., DUNCOMBE, P., GUPTA, A. & LAIBOWITZ, R. (1997). Temperature dependent, non-ohmic magnetoresistance in doped perovskite manganate trilayer junctions. *Appl. Phys. Lett.* **70,** 1769-1771.

TAFTO, J. and KRIVANEK, O. L. (1982). Site-Specific Valence Determination by Electron Energy-Loss Spectroscopy. *Phys. Rev. Lett.* **48,** 560-563.

TAN, H., VERBEECK, J., ABAKUMOV, A. & VAN TENDELOO, G. (2012). Oxidation state and chemical shift investigation in transition metal oxides by EELS. *Ultramicroscopy* **116,** 24-33.

TURQUAT, C., LEROUX, C., GLOTER, A., SERIN, V. & NIHOUL, G. (2001). V-doped HfO_2: thermal stability and vanadium valence. *Int. J. Inorg. Mater.* **3,** 1025-1032.

VAN AKEN, P. A., LIEBSCHER, B. & STYRSA, V. J. (1998). Quantitative determination of iron oxidation states in minerals using Fe $L_{2,3}$ -edge electron energy-loss near-edge structure spectroscopy. *Phys. Chem. Miner.* **25,** 323-327.

VARELA, M., OXLEY, M. P., LUO, W., TAO, J., WATANABE, M., LUPINI, A. R., PANTELIDES, S. T. & PENNYCOOK, S. J. (2009). Atomic-resolution imaging of oxidation states in manganites. *Physical Review B* **79,** 085117.

WANG, Y. Q., MACLAREN, I. & DUAN, X. F. (2001). EELS analysis of manganese valence states in rare-earth manganites $(La_{1-x}Y_x)_{0.5}(Ca_{1-y}Sr_y)_{0.5}MnO_3$. *Mat. Sci. Eng. A* **318,** 259-263.

ZHANG, S., LIVI, K. J. T., GAILLOT, A., STONE, A. T. & VEBLEN, D. R. (2010). Determination of manganese valence states in (Mn(3+), Mn(4+)) minerals by electron energy-loss spectroscopy. *Am. Mineral.* **95,** 1741-1746.